scientific reports

OPEN

First observation of fluid-like eddy-dominant bursty bulk flow turbulence in the Earth's tail plasma sheet

L. Q. Zhang[1], Chi. Wang[1✉], W. Baumjohann[2], R. S. Wang[3], J. Y. Wang[4], James L. Burch[5] & Yu. V. Khotyaintsev[6]

Turbulence is a ubiquitous phenomenon in neutral and conductive fluids. According to classical theory, turbulence is a rotating flow containing vortices of different scales. Eddies play a fundamental role in the nonlinear cascade of kinetic energy at different scales in turbulent flow. In conductive fluids, the Alfvénic/kinetic Alfvénic wave (AW/KAW) is the new "cell" of magnetohydrodynamic (MHD) turbulence (frozen-in condition). Wave energy, which has equal kinetic and magnetic energy, is redistributed among multiple-scale Fourier modes and transferred from the large MHD scale to the small kinetic scale through the collision of counter-propagating Alfvénic wave packages propagating along the magnetic field line. Fluid-like eddy-dominant plasma flow turbulence has never been found in space since the launch of the first satellite in 1957. In this paper, we report the first observation of eddy-dominant turbulence within magnetic reconnection-generated fast flow in the Earth's tail plasma sheet by the Magnetospheric Multiscale Spacecraft (MMS). In eddy-dominant turbulent reconnection jet, ions dominate the flow field while electrons dominate current and magnetic fluctuations. Our findings shed new light on the nonlinear kinetic and magnetic energy cascade in MHD turbulence.

Magnetic reconnection occurs extensively in space, including on the surface of the Sun, in the magnetosheath region, and at the Earth's dayside magnetopause and nightside magnetotail[1–3]. During the magnetic reconnection, the magnetic energy stored in the stretched thin current sheet is rapidly released and converted to kinetic energy. The fast flow generated during reconnection in the Earth's magnetotail is also known as bursty bulk flow (BBF)[4–6]. BBF has been widely observed in the tail plasma sheet from the near-Earth region of $\sim 7~R_E$ (R_E is the earth radius) to downtail beyond 100 R_E[7,8].

The BBF in the plasma sheet is a short-lived turbulent flow that lasts for several minutes to tens of minutes[9–11]. Typically, the BBF is convective in the central plasma sheet (CPS) when $\beta > 1$ (where β is the ratio of thermal pressure to magnetic pressure), and field-aligned near the plasma sheet boundary layer (PSBL) when $0.1 < \beta < 1$[12,13]. In the vicinity of the reconnection region, the speed of the BBF can reach up to ~ 1000 km/s. However, after leaving the reconnection source region, the BBF may experience significant deceleration, slowing down to several hundred kilometers per second before reaching the braking region around $\sim 10~R_E$[14,15].

The BBF is intrinsically a turbulent plasma flow with superimposed eddies and waves. Magnetic fluctuations during the BBF demonstrate enhanced wave activities within the turbulence[16–19]. Simultaneous measurements of electric and magnetic fluctuations show an increase in the parallel-predominantly Poynting flux ($\mathbf{P} = \Delta\mathbf{E} \times \Delta\mathbf{B}$) and power spectral ratio $|\Delta E|/|\Delta B|$ during the BBF interval. These features are consistent with those of the kinetic Alfvénic wave (KAW)[20,21]. Additionally, compressible fluctuations induced by slow-mode waves are also found within the turbulent BBF[22,23].

Early research on velocity fluctuations in the tail plasma sheet revealed the formation of coherent vorticity ($\boldsymbol{\omega} = \nabla \times \mathbf{V}$, where V is the velocity of the mass center of the fluid element) and large-scale vortex structures[24–28]. Recent direct measurements of plasma vorticity based on four-point joint observations by MMS spacecraft

¹State Key Laboratory of Space Weather, National Space Science Center, Chinese Academy of Sciences, Beijing 100080, China. ²Space Research Institute, Austrian Academy of Sciences, 8042 Graz, Austria. ³CAS KCAS Key Laboratory of Geospace Environment, Department of Geophysics and Planetary Science, University of Science and Technology of China, Hefei 230026, China. ⁴Information Engineering College, Central University for Nationalities, Beijing 100081, China. ⁵Southwest Research Institute San Antonio, San Antonio, TX 78238, USA. ⁶Swedish Institute of Space Physics, Uppsala, Sweden. ✉email: cw@nssc.ac.cn

1

have exhibited an enhancement in ω within the turbulent BB[29,30]. The ω-field in the course of the BBF exhibits perpendicular-anisotropy. In particular, low-frequency fluctuations in the ω-field show a good correlation with the flow speed of the BBF. The higher the flow velocity, the greater the vorticity. The properties of vorticity, namely convective or kinetic, depends on the flow filed of the BBF. Kinetic BBF tends to have stronger vorticity than convective BBF[31].

In this paper, we analyze the velocity and magnetic fluctuations observed within the BBF observed on Aug 16, 2018, by the MMS spacecraft. MMS mission[32] consists of four identical spacecraft, with high-accuracy measurements of plasma moments and small spacecraft separations of tens of kilometers. The MMS data has 0.125-s resolution for Fluxgate magnetometers (FGM)[33], 4.5-s resolution for Fast Plasma Investigation (FPI)[34], and 0.03-s resolution for Electric Field Double Probe (EDP)[35]. Geocentric Solar Magnetospheric (GSM) coordinate system is adopted. During this event, the BBF near the PSBL lasted for 22 min and had an average flow velocity of 312 km/s ($V_A = 937$ km/s, and $V_A = \pm B_0(\mu_0\rho)^{-1/2}$ is Alfvénic velocity), making it a sub-Alfvénic flow. The velocity fluctuations exhibited parallel-anisotropy ($\Delta V_{//}/\Delta V_\perp \sim 2.1$) and had low correlation with the magnetic fluctuations. The ω-field in the course of the BBF is perpendicular-predominantly. In particular, the spectra of magnetic field B and current J demonstrate dissipation scaling in the inertial range (below ion gyrofrequency). These observations offer a new perspective on the kinetic energy cascade and dissipation by eddies in magnetohydrodynamic (MHD) turbulence.

A scenario of eddy and wave contributions to the velocity fluctuations within BBF turbulence

The scenario of velocity fluctuations in the BBF turbulence at the boundary layer of the plasma sheet is illustrated in Fig. 1. After leaving the reconnection source region, the BBF moves earthward. In the center of the BBF, the current sheet typically has a significant normal field ((B_z) and/or dawn-dusk field (B_y), resulting in mainly convective motion in the CPS. However, at the plasma sheet boundary layer, the B_x component becomes dominant, causing the BBF to become field-aligned and move along the background magnetic field lines $\mathbf{B_0}$ (Panel A).

Eddies and waves coexist in the BBF (Panel B). Eddies of various scales are frozen in the BBF and move together (based on the Taylor hypothesis). These eddies contribute to the velocity fluctuations in the flow field of the BBF. Alfvén waves travel through the BBF at an Alfvénic speed along the B_0 and contribute to magnetic and velocity fluctuations, both in the perpendicular direction relative to B_0 (Panel C). Compressible modes may also exist, causing perpendicular fluctuations in the flow field and parallel fluctuations in the magnetic field. The rotating eddies cause enhanced ω within the BBF, primarily in the perpendicular direction relative to the background flow or, equivalently, the magnetic field (Panel E). Considering that only eddy contributes to parallel fluctuation $\Delta V_{//}$, there has,

$$\Delta \mathbf{V}_{//} = \mathbf{V}_{//\text{eddy}}, \tag{1}$$

$$\Delta \mathbf{V}_\perp = \Delta \mathbf{V}_{\perp\text{eddy}} + \Delta \mathbf{V}_{\perp\text{wave}}. \tag{2}$$

The Alfvénic perturbations satisfy the relationship: $\Delta \mathbf{E} + \Delta \mathbf{V}_{\perp\text{wave}} \times \mathbf{B}_0 = 0$ and $\frac{\Delta E}{\Delta B_\perp} = V_A$. Here $\Delta \mathbf{E}$ is the perturbed electric field. Simple calculation yields that: $\Delta \mathbf{V}_{\perp\text{wave}} = \frac{\Delta \mathbf{B}_\perp}{B_0} V_A$. Inserting it into Eq. (2), we obtain

$$\frac{\Delta \mathbf{V}_\perp}{V_A} = \frac{\Delta \mathbf{V}_{\perp\text{eddy}}}{V_A} + \frac{\Delta \mathbf{B}_\perp}{B_0}. \tag{3}$$

The first and second terms at the left hand represent the contributions of eddy and wave to $\Delta V_\perp$, respectively.

Defining parallel Alfvén Mach number $M_{A//} = \frac{|\delta V_{//}|}{V_A}$ and perpendicular Alfvén Mach number $M_{A\perp} = \frac{|\delta V_\perp|}{V_A}$, the MHD turbulence is eddy-dominant if $M_{A//} > M_{A\perp}$ and/or $M_{A\perp} > \frac{\Delta B_\perp}{B_0}$. Else, the MHD turbulence is wave-dominant.

Event on Aug 16, 2018
Overview

Figure 2 shows the temporal evolution of ion and magnetic field measurements obtained by the FPI and FGM instruments onboard the MMS1 spacecraft from 05:45 to 06:35 UT. The trajectory and separation distance of the MMS spacecraft are also shown. The MMS spacecraft is initially located in the dusk-side plasma sheet around $(-22.5 R_E, 9.1 R_E, 4.5 R_E)$. The separation distance between the MMS1 and MMS2 (MMS3) spacecraft is 17 km in the X–Y plane, while the separation distance between MMS1 and MMS4 is 2 km in the X–Y plane. In the X–Z plane, the separation distance between MMS1 and MMS2 (MMS3) is 20 km, while the separation distance between MMS1 and MMS1 is 31 km in the same plane.

The BBF begins at 05:58 UT and ends at 06:21 UT, as indicated by the two vertical lines in the figure. During this time, the MMS spacecraft moves slowly radially towards Earth (Panel K) and towards the equator in the north–south direction (Panel L). Prior to the appearance of the BBF, the plasma sheet is slightly flapping, and the MMS1 spacecraft gradually moves towards the CPS. Upon entering the BBF, the spacecraft moves towards the inner PSBL, where the ion density is approximately ~ 0.3 cm^{-3} and the ion temperature is approximately 3 keV. At 06:04 UT, MMS1 briefly enters the CPS and then returns to the inner plasma sheet.

The BBF is a sub-Alfvénic flow with an average velocity of 312 km/s ($V_A = 937$ km/s). The flow field in the course of the BBF is highly structured, with opposing flows against the BBF on a temporal scale of 1–3 min (marked by shadows). In the normal flow field of the BBF (outside the shadows), the velocity fluctuates strongly, and the ω field shows significant enhancement. In contrast, the opposing flow with large negative V-fluctuation ($\Delta V < 0$) has only slight velocity fluctuations and no ω-enhancement. The ion population (Panel A) exhibits subtle variations in the opposing flows of higher-β and lower-β. The lower-β opposing flow (yellow shadow) has
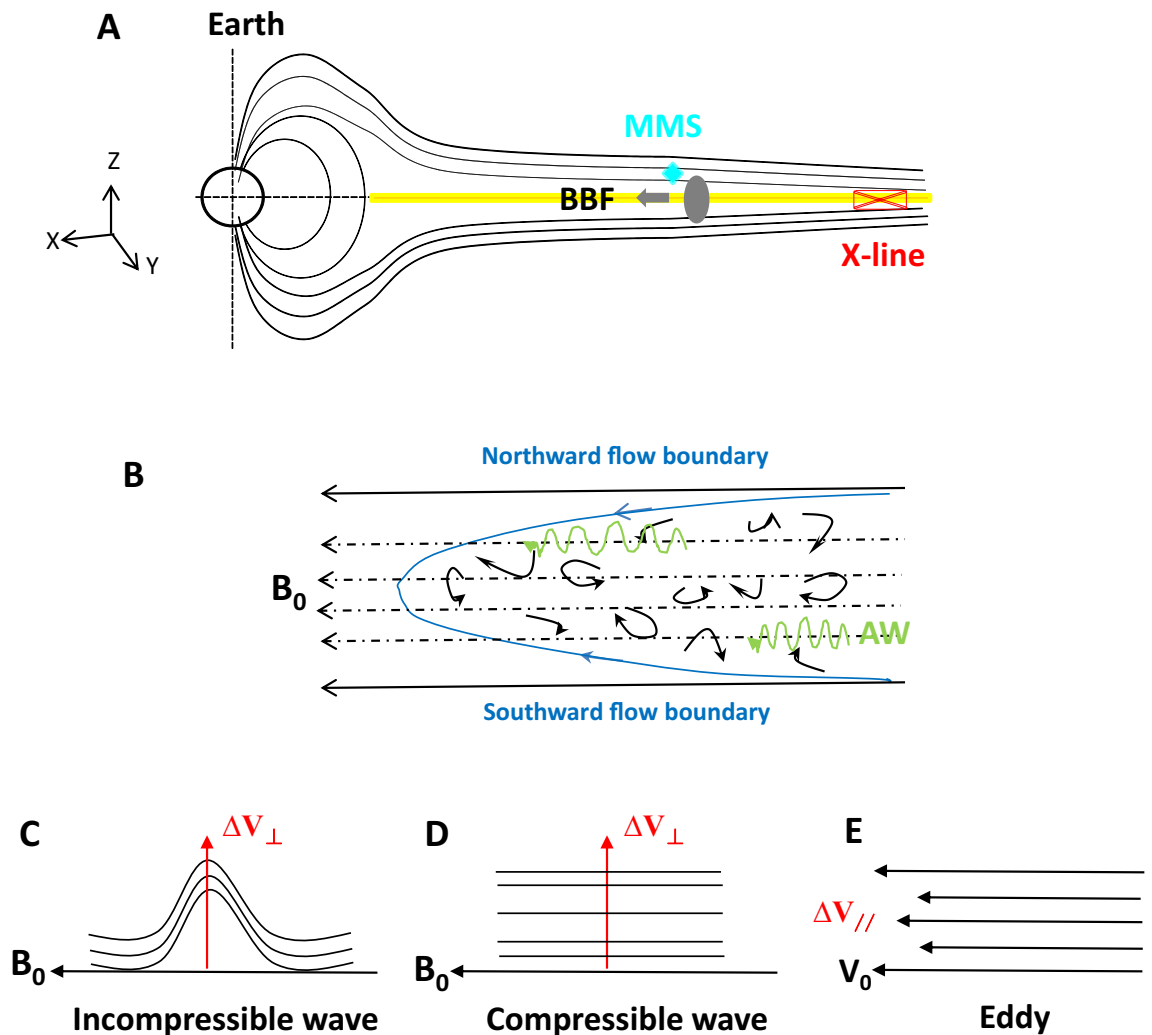
Figure 1. Schematic diagram of the field-aligned BBF turbulence superimposing eddy and wave at the PSBL away from the reconnection source region. (**A**) Is a schematic of the earthward-moving BBF along the background magnetic field at the inner PSBL (Geocentric solar magnetospheric (GSM) coordinates are adopted). The yellow region marks the cross-tail current sheet at the center of the tail plasma sheet, and the X-line denotes the location of the reconnection source region. MMS is located in the northward hemisphere and encounters the turbulent BBF near the PSBL. (**B**) Depicts the scenario of eddies of different scales within the BBFs. The black solid straight line with an arrow represents the magnetic field lines at the flow boundaries in the north and south hemispheres, and the dashed straight line with an arrow represents the magnetic field line internal to the BBF. Blue represent flow boundary. Green represents Alfvénic waves along the background magnetic field. Near the flow boundary, the flow and background field are both earthward, and the eddies are frozen in the flow, moving with the BBF together. The AW travels through the BBF along the B_0. (**C**) Shows the perpendicular velocity and magnetic fluctuations caused by the Alfvénic mode. (**D**) Shows the perpendicular velocity fluctuation and parallel magnetic fluctuations caused by compressible modes. (**E**) Depicts the parallel velocity fluctuation ($\Delta V_{//}$) caused by eddies.

stronger B and lower n/T and corresponds to a decrease in ion flux at high-energy (above 10 keV) in the ion energy spectrum. The higher-β opposing flow (grey shadows) has weaker B and higher n/T and corresponds to an increase in ion flux in low and medium energy (500 eV–5 keV). The opposing flow of mixed different ion populations is consistent with the passage of large-scale Kelvin–Helmholtz vortex structures[36,37].

Parallel-anisotropic velocity fluctuation

Unperturbed and perturbed fluctuations in the flow and magnetic fields during the BBF interval are shown in Fig. 3. The BBF turbulence exhibits a quiet background. From Panel B, it can be seen that the background magnetic field is dominated by the B_{x0} component, which slowly decreases from 28.4 to 22.3 nT, with an average value of 23.7 nT. In comparison, the B_{y0} and B_{z0} components are small and unclear, indicating that the background plasma sheet is in a quiet state. This rules out the potential influence of plasma sheet motion on the BBF turbulence, such as tilting, twisting, and flapping. The V_{x0} component remains steady at 304 km/s ($V_A = 937$ km/s), with
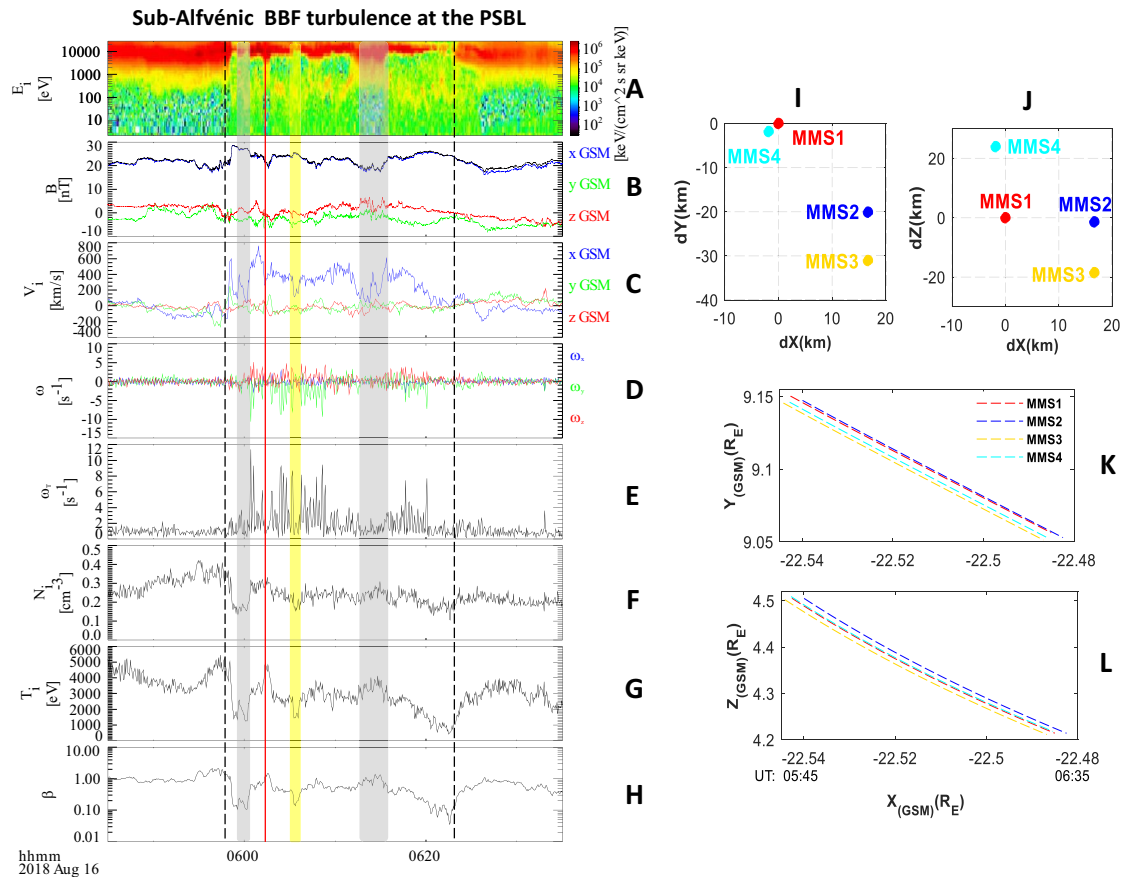
Figure 2. Overview on sub-Alfvénic BBF turbulence at the boundary layer of the plasma sheet observed by MMS1 spacecraft. The left column shows the temporal evolution of the turbulent BBF. (**A**) Ion energy spectrum. (**B**) Bx, By, and Bz. (**C**) Vx, Vy, and Vz. (**D**) ω_x, ω_y and ω_z. (**E**) Total ω ω_T. (**F**) Ion density n_i. (**G**) Ion temperature T_i. (**H**) Plasma β. The right column is the orbit of the MMS. Panels (**I,J**) show the distances between MMS1 and the other three MMS satellites in the X–Y and X–Z planes, respectively. Panels (**K,L**) show the trajectories of MMS from 05:30 to 06:30 UT in the X–Y and X–Z planes, respectively. The BBF lasts from 05:58 to 06: 21 UT (between the two vertical lines). Shadows mark the opposite flow of the low-ω superimposed on the normal flow of the BBF. The grey shadows are the opposite flows of higher-β, and yellow shadow is the opposite flows of lower-β. The red vertical line marks the short dip of MMS1 into the CPS at 06:04 UT.

small fluctuations in V_{y0} and V_{z0}. The average angle between V_0 and B_0 is approximately 2.7°, indicating that the background flow of the BBF is quasi-parallel, moving along the background magnetic field.

Panel E shows that the velocity fluctuation in the turbulent flow field exhibits a prominent parallel-anisotropy ($\Delta V_{//}/\Delta V_\perp \sim 2.1$), with an average value of $\Delta V/V_0$ over the BBF time of ~ 0.5. The Mach number ($M_A = V/C$, where V is flow velocity and C is speed of sound)) is ~ 0.15. The magnetic fluctuation in the BBF is slight ($\Delta B/B_0 \sim 0.16$), without clear preference in parallel and perpendicular directions ($\Delta B_{//}/\Delta B_\perp \sim 1.0$). The ω-field of the eddy-dominant BBF is perpendicular-predominantly.

To clarify the contributions of eddies and waves to BBF turbulence, we further compare the different terms in Formula (3). Panel (I) displays $M_{A//}$, $M_{A\perp}$, and R_B ($= \Delta B_\perp/B_0$). Throughout the BBF interval, R_B remains small. $M_{A//}$ is mostly much greater than $M_{A\perp}$, and both are much greater than R_B. Clearly, eddy dominates the velocity fluctuation in the flow field of the BBF, as opposed to wave. At the end of the BBF, R_B becomes the greatest, indicating that wave fluctuations dominate the post-BBF flow.

E-fluctuations and wave activities

The associated evolutions of **E**-field and Poynting flux (**P**) from 05:40 to 06:30 UT are plotted in Fig. 4. All components in the E-field fiercely fluctuate, with spikes of 10–20 mV/m. Despite the spikes, the E-field is composed of a superimposition of slowly-varying convective-**E** (E_c) and rapidly-varying kinetic-**E** (E_k), with E_c being the main component. The net E·J over the BBF time is negative (− 0.9), suggesting a Joule dissipation of the BBF.

The Poynting flux shows a substantial enhancement within the BBF, with the enhanced-P having a higher parallel component ($P_{//}$) than the perpendicular component ($P_\perp$). The maximum magnitude of $P_{//}$ is ~ 0.06 erg cm^{-2} s^{-1}. Notably, the strengths of P in the normal flow (outside shadows) and opposite flow (inside shadows) show no distinct difference. This implies that the AW/KAW activities during the course of the BBF may not be directly related to the ω-field.

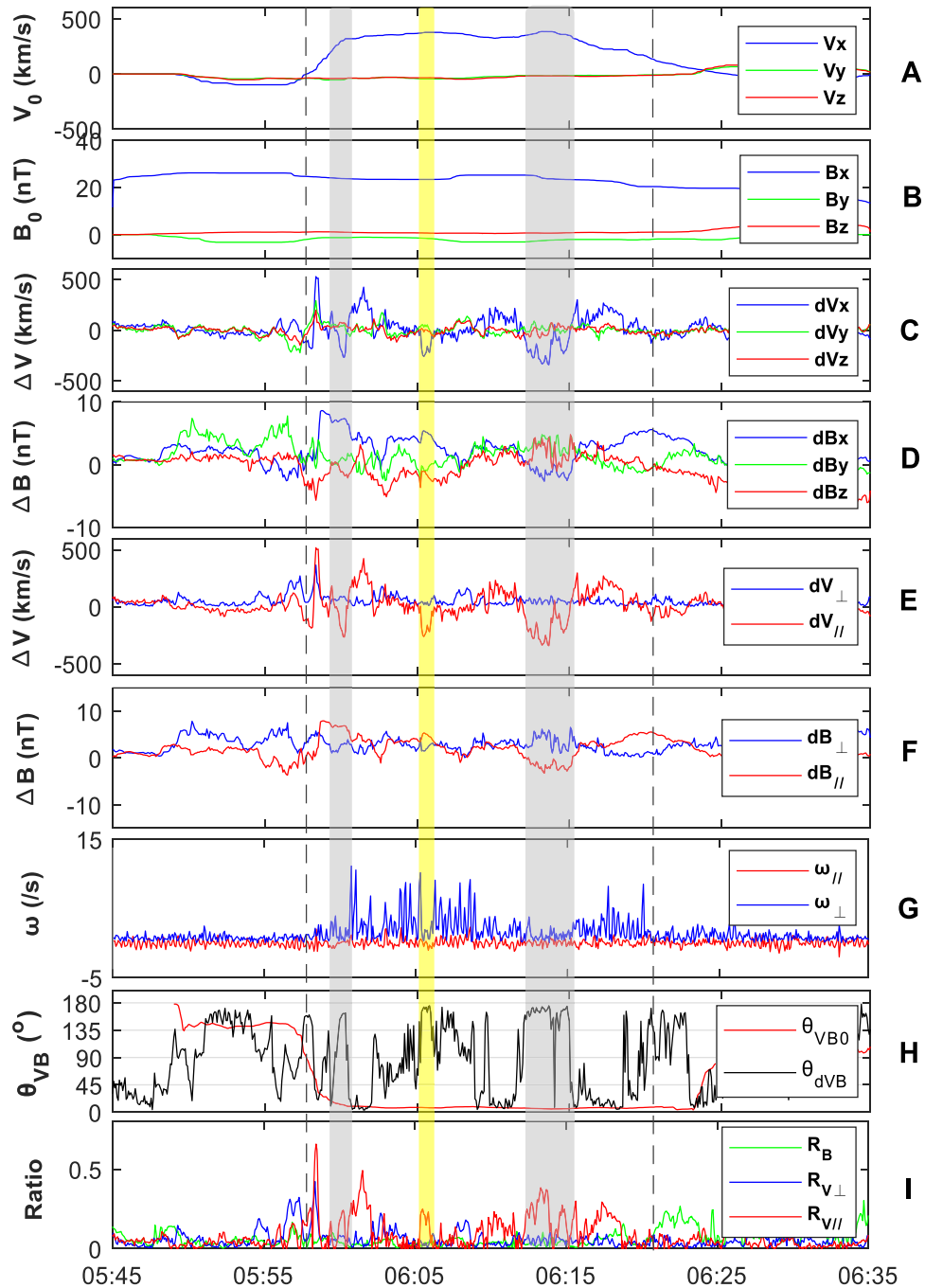## Parallel-predominantly velocity fluctuations within the BBF

Figure 3. Perturbed and unperturbed fluctuations in the flow and magnetic fields during the interval of the parallel BBF near the PSBL observed by MMS1. (**A**) V_{x0}, V_{y0}, and V_{z0}. (**B**) B_{x0}, B_{y0}, and B_{z0}. (**C**) ΔV_x, ΔV_y, and ΔV_z. (**D**) ΔB_x, ΔB_y, and ΔB_z. (**E**) $\Delta V_{//}$ and $\Delta V_\perp$. (**F**) $\Delta B_{//}$ and $\Delta B_\perp$. (**G**) $\omega_{//}$, and $\omega_\perp$. (**H**) θ_{VB0} ($=\arctan(V_0/B_0)$) and θ_{dVB} ($=\arctan(\Delta V/B_0)$) (**I**) R_B ($=\Delta B_\perp/B_0$), $Rv_{//}$ ($=\Delta V_{//}/V_A$) and $Rv_\perp$ ($=\Delta V_\perp/V_A$). The median filter with a cutoff frequency of 0.015 Hz is applied to separate the unperturbed and perturbed components in the velocity and magnetic fields. The high-resolution magnetic field data (B-data) is interpolated to match the FPI-data. Subsequently, the interpolated magnetic field data is used to calculate the perturbed and unperturbed $V_{//}/\omega_{//}$ and $V_\perp/\omega_\perp$ components. The shadows are the same as in Fig. 2.

The correlation coefficient (CC) between velocity and magnetic fluctuations is shown in Panels F–H. During the BBF interval, the CC is 0.04 between ΔV_x and ΔB_x, 0.05 between ΔV_y and ΔB_y, and 0.03 between ΔV_z and ΔB_z.
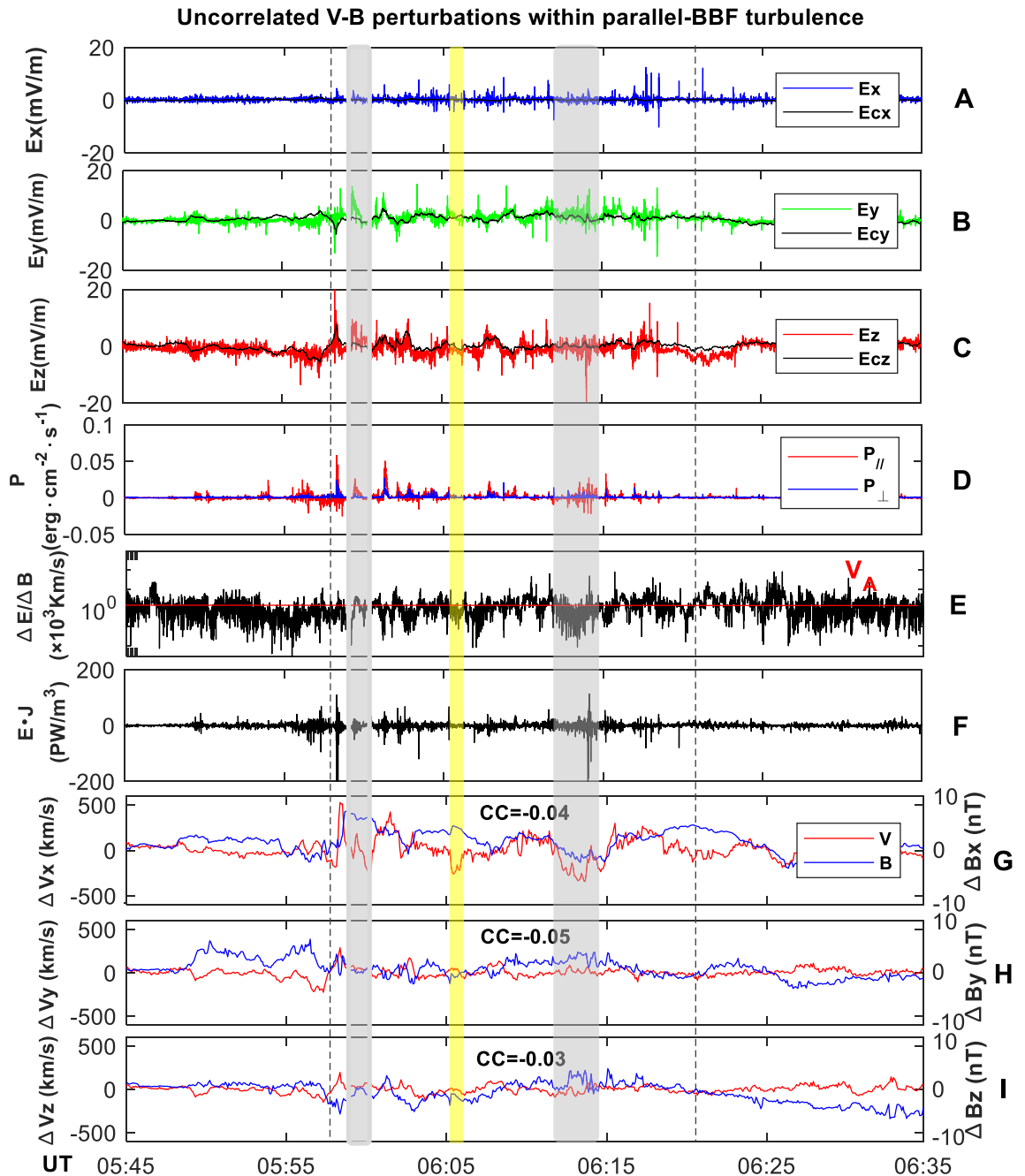
Figure 4. E-fluctuation and wave actives within eddy-dominant BBF turbulence. (**A**) Measured Ex vs. Ecx. (**B**) Measured Ey vs. Ecy. (**C**) Measured Ez vs. Ecz. (**D**) $P_{//}$ and $P_\perp$. (**E**) $|\Delta E_\perp/\Delta B_\perp|$. (**F**) E·J. ΔB_z. (**G**) ΔV_x vs. ΔB_x. (**H**) ΔV_y vs. ΔB_y. (**I**) ΔV_z vs. ΔB_z. To obtain the convective and kinetic E ($E_k = E + E_c$, and $Ec = V \times B$), the original E and **B** data are all interpolated too match the 4.5 s time cadence of the FPI data. The interpolated **E/B** data is then used to calculate the **Ec** and **E$_k$**. To calculate the Poynting flux, the original **E**-data is interpolated to match the **B**-data. The electric and magnetic fields data from the EDP and FGM instruments onboard MMS1 are detrended by a 10-min-window running average. The perturbed **E** and **B** fields are then used to calculate the Poynting vector (**P** $= \Delta E \times \Delta B$). To accurately calculate the correlation coefficient (CC) in Panels (**F–H**), only data during the BBF-time are used. A total of 304 data points are collected (from 05:58 to 06:21).

The CC between ΔV and ΔB is evaluated to be ~0.2. The low correlation indicates that within the eddy-dominant BBF, magnetic and velocity fluctuations are non-Alfvénic in nature.

Non-Kolmogorov spectrum and electron dynamic

Figure 5A illustrates the power spectrum of the $\Delta B_{//}$ and $\Delta B_\perp$. Below 0.3 Hz (ion gyrofrequency, f_{gy}), the B-spectrum deviates significantly from Kolmogorov's $-5/3$ law. The scaling of the spectra of $\Delta B_{//}$ and $\Delta B_\perp$ is similar, approximately -2.5. Above 0.3 Hz, the scaling of the $\Delta B_{//}$-spectrum remains the same, whereas the scaling of the

$\Delta B_\perp$-spectrum becomes -2.7, indicating faster dissipation of magnetic energy in the perpendicular direction than in the parallel direction.

The spectra of $J_{//}$ and $J_\perp$ are shown in Panel (B). Similarly, the J-spectrum deviates from Kolmogorov's $-5/3$ law in the inertial regime. At 0.28 Hz, a deep dip appears in the $\Delta J_\perp$-spectrum. The dip in the $\Delta J_{//}$-spectrum is ambiguous. In the low-frequency subrange, the $J_\perp$-spectrum rises from ~ 10 $(nA/m^2)^2/Hz$ at 0.03 Hz to ~ 20 $(nA/m^2)^2/Hz$ at 0.05 Hz. Above 0.05 Hz, the $J_\perp$-spectrum is straight with a slope of about -2.5. Below 0.05 Hz, the $J_{//}$-spectrum is flat. From 0.05 Hz to 0.1 Hz, the spectrum of the $J_{//}$ slowly decrease from ~ 70 $(nA/m^2)^2/Hz$ to ~ 50 $(nA/m^2)^2/Hz$. Above 0.1 z, the $J_{//}$-spectrum has a dissipation scaling of -3-like.

Panel (C) shows probability density distributions (PDD) of $\Delta B_{//}$ and $\Delta B_\perp$. The distribution of the $\Delta B_\perp$ deviates from the Gaussian distribution with a clear tendency. When $|\Delta B_\perp| < 1.5$ nT, the $|\Delta B_\perp|$ is lower than the Gaussian fitting result, while when $|\Delta B_\perp| > 1.5$ nT, it is higher than the result of Gaussian fitting result. In contrast, the distribution of $\Delta B_{//}$ is basically symmetric. When $|\Delta B_{//}| < 1.5$ nT, $\Delta B_{//}$ basically follows Gaussian distribution. However, when $|\Delta B_{//}| > 1.5$ nT, it is distinctly higher than the expect value of Gaussian fitting. For both $\Delta B_{//}$ and $\Delta B_\perp$, the greater fluctuation has a higher probability, which is consistent with the intermittence characteristic. Therefore, the intermittent turbulence is a likely explanation for the non-Kolmogorov spectra of $\Delta B_{//}$ and $\Delta B_\perp$ in the inertial subrange[38–40].

The temporal evolution of electron velocity (measured by FPI) and momentum current from 05:58 to 06:21 UT are shown in Panels (D-G). Momentum current J is calculated by $J = n_i e\,(V_i - V_e)$, where the subscript i and e represents ion and electron, respectively, n_i is the ion density, and e is the ion charge. For all components, V_e fluctuated fiercely, and it is about an order of magnitude higher than V_i. Thus, ions and electrons are decoupled
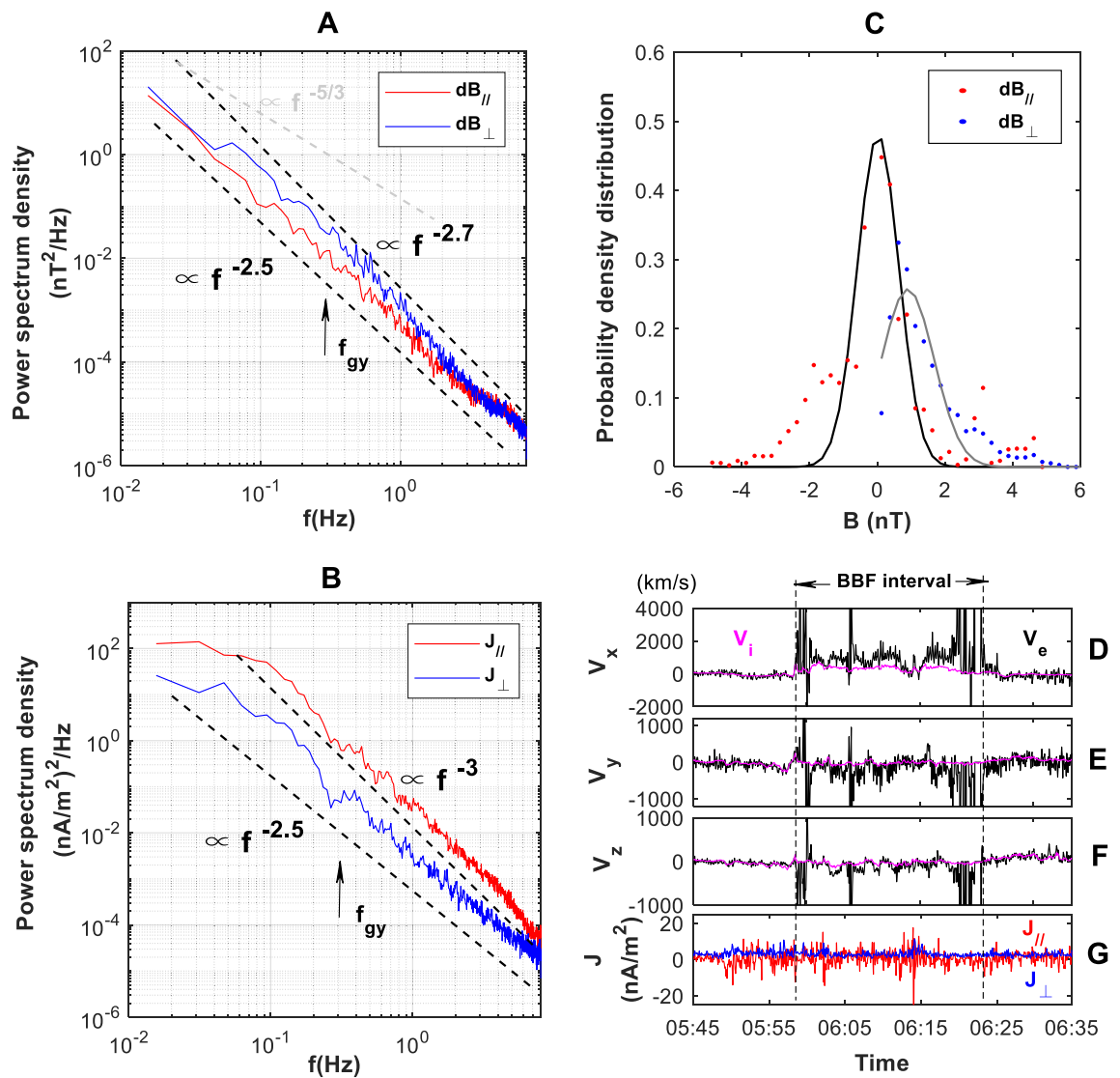

Figure 5. Spectrum and electron dynamic in the eddy-dominant BBF turbulence. Ion gyro-frequency f_{gy} is 0.3 Hz. (**A**) Spectra of $\Delta B_{//}$ and $\Delta B_\perp$. (**B**) Spectra of $J_{//}$ and $J_\perp$ (calculated by $\nabla \times B/\mu_0$). (**C**) Power density probability of the $\Delta B_{//}$ and $\Delta B_\perp$. The lines are fitted with a single Gaussian (black and grey) that provides an estimate of intermittency in BBF turbulence. (**D**) v_{ix}, v_{ex}. (**E**) v_{iy}, v_{ey}. (**F**) v_{iz}, v_{ez}. (**G**) $J_{//}$ and $J_\perp$ (calculated by $\nabla \times B/\mu_0$).

in their macroscopic fluid behavior. Electron dominates the turbulent current **J**. Panel G shows that the electron-dominated **J** has a greater parallel component ($J_{//}$) than perpendicular component ($J_{\perp}$) which accounts for the $J_{//}$ being higher than $J_{\perp}$ in Panel B.

Eddy-dominant BBF on July 30, 2017

To verify the non-Kolmogorov spectrum, we present another eddy-dominant BBF observed at the PSBL on July 30, 2017. The two BBFs have similar properties in their flow and magnetic fields. The temporal evolutions of the flow and magnetic fields from 06:05 to 06:35 UT are shown in Fig. 6 (right column). MMS1 is initially posited in the midnight near-Earth plasma sheet at ($-16.5\ R_E$, $2.0\ R_E$, $4.7\ R_E$). The BBF appears at 06:09 UT and lasts until 06:28 UT. The average velocity of the BBF is ~ 155 km/s, and the maximum velocity is 423 km/s ($V_A = 1066$ km/s). Therefore, the BBF is a sub-Alfvénic flow. The V_x component dominated the flow field, and the B_x component dominated the magnetic field. The B_y and B_z components in the background plasma sheet were quite weak. The flow field is highly turbulent ($\Delta V/V_0 \sim 0.8$). The velocity fluctuation in the turbulent flow field is parallel-anisotropic ($\Delta V_{//}/\Delta V_{\perp} \sim 1.9$), with a low correlation with the magnetic fluctuation ($CC = 0.06$). Thus, the BBF is dominated by the eddy. The magnetic turbulent fluctuation was parallel-anisotropic ($\Delta B_{//}/\Delta B_{\perp} \sim 1.9$). Additionally, the eddy-dominant BBF has a stronger $J_{//}$ component than the $J_{\perp}$ component (calculated by $\nabla \times \mathbf{B}/\mu_0$, where μ_0 is the magnetic permeability of the plasma).

The power spectra of B and J are shown in Panels A and B. In the low-frequency subrange, both parallel and perpendicular spectra of **B** as well as **J** deviate from Kolmogorov's $-5/3$ law, in a similar dissipative slope. In the high-frequency subrange, the slope of the $\Delta B_{\perp}$-spectrum is steeper than the $\Delta B_{//}$-spectrum, while the slope of the $J_{//}$-spectrum is steeper than the $J_{\perp}$-spectrum.
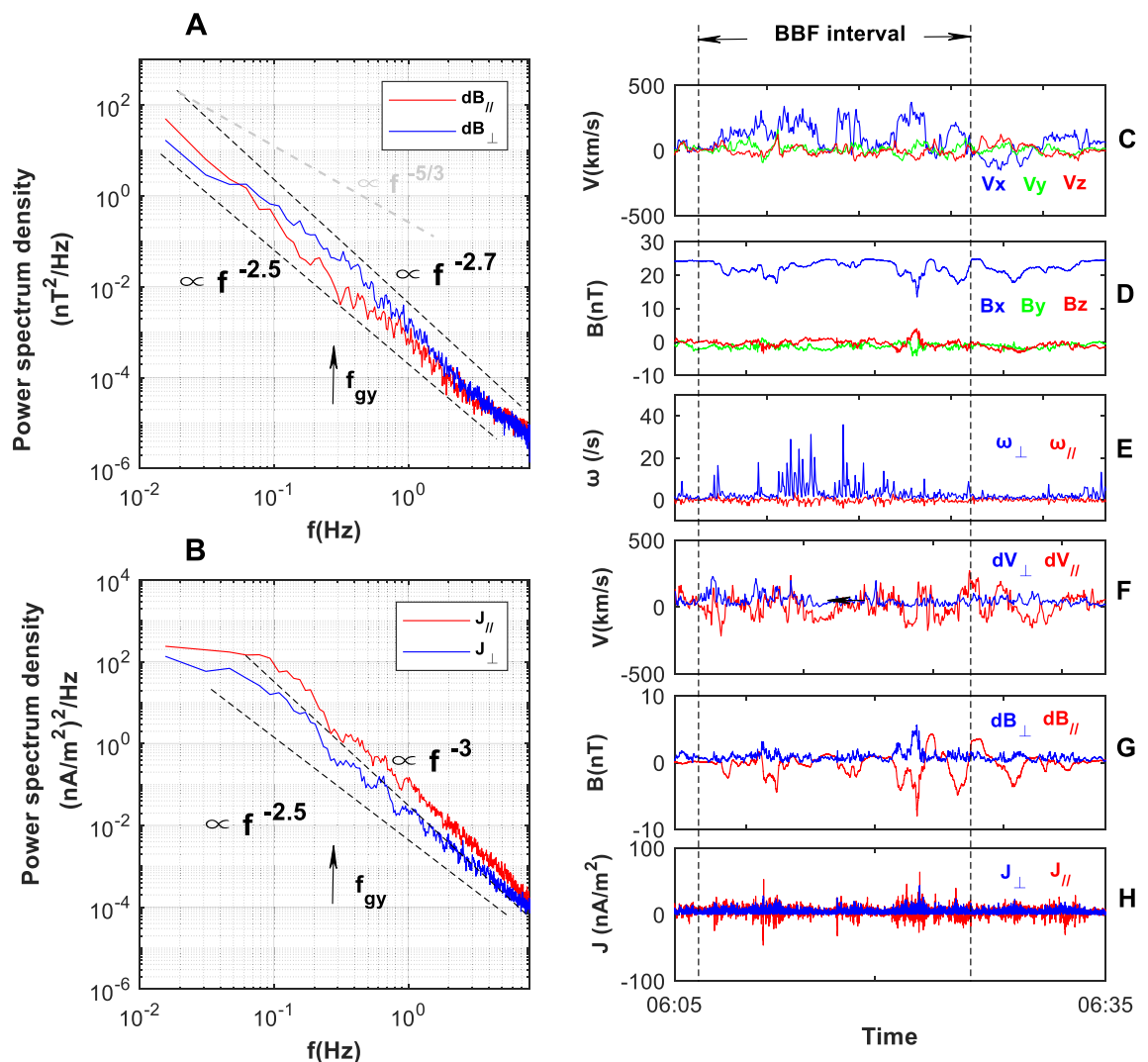

Figure 6. Spectral of B and J in the eddy-dominant BBF turbulence at the PSBL on July 30, 2017 observed by MMS1. The BBF lasts from 06:09 to 06:28 (within the two vertical lines). Left column is power spectra. (**A**) Spectra of $\Delta B_{//}$ and $\Delta B_{\perp}$. (**B**) Spectra of $J_{//}$ and $J_{\perp}$. Right column is the evolution of the flow and magnetic field in the course of the BBF. (**C**) Vx, Vy, and Vz (from ion measurement by FPI). (**D**) Bx, By, and Bz. (**E**) $\omega_{//}$, and $\omega_{\perp}$. (**F**) $\Delta V_{//}$ and $\Delta V_{\perp}$. (**G**) $\Delta B_{//}$ and $\Delta B_{\perp}$. (**H**) $J_{//}$ and $J_{\perp}$ ($\mathbf{J} = \nabla \times \mathbf{B}/\mu_0$).

Comparing Figs. 5 and 6, the main spectra characteristics of two BBFs are similar, including their spectral intensities and slopes. This similarity suggests that the non-Kolmogorov spectra in the inertial range are not accidental. In the eddy-dominant BBF, both eddy and wave can subtract energy from magnetic field. As a result, magnetic energy dissipation may be faster than predicted by Kolmogorov's $-5/3$ law. This may be responsible for the dissipative scaling of the **B** and **J** spectra in the inertial range.

Eddy-dominant MHD turbulence: physics and implication

Near the PSBL, the magnetic field is strong, and the plasma tends to move along the magnetic field. In this case, the fluid-like flow turbulence may occur, in which the flow fluctuates mainly along the background flow as if the magnetic field does not exist.

The Alfvénic speed near the PSBL is typically of ~ 1000 km/s. While propagating through the BBF of several hundred kilometers per second, the difference in velocities of wave and flow results in a large "Doppler shift", causing the wave to be non-resonant with the turbulent eddies. This non-resonance prevents the wave from interacting with the turbulence, as the turbulence is not able to effectively "catch up" with the wave. As a consequence, the eddy overwhelms the wave and dominates the flow within the BBF.

Unlike Alfvénic vorticity in the wave turbulence[41–44], the eddy vorticity in the BBF turbulence is perpendicular-predominantly. The presence of non-Alfvénic vorticity in the BBF implies that there are independent kinetic and magnetic cascades occurring in MHD turbulence[45–47]. That is to say, the kinetic and magnetic cascades are not strongly coupled and can evolve independently of each other within BBF turbulence.

Summary

In summary, eddies dominate over wave within the parallel BBF at the PSBL, resulting in velocity fluctuations that are primarily parallel and have low correlation with magnetic fluctuations. The ω-field in the eddy-dominant BBF is predominantly perpendicular. While ions dominate the flow field, electrons dominate current and magnetic fluctuations. Specifically, at low frequencies, the spectra of both magnetic field and current exhibit non-Kolmogorov scaling in the inertial range. At high frequencies (above the ion gyrofrequency), the $B_\perp$-spectrum has a steeper slope than the $B_{//}$-spectrum, while the $J_{//}$-spectrum has a steeper slope than the $J_\perp$-spectrum.

Data availability

The datasets analyzed during the current study are available in the [CDAWEB] repository, [https://cdaweb.gsfc.nasa.gov/pub/data/mms/].

References

1. Dungey, J. W. Interplanetary magnetic fields and the auroral zones. *Phys. Rev. Lett.* **6**, 47–48. https://doi.org/10.1103/PhysRevLett.6.47 (1961).
2. Øieroset, M., Phan, T. D., Fujimoto, M., Lin, R. P. & Lepping, R. P. In situ detection of collisionless reconnection in the Earth's magnetotail. *Nature* **412**, 414. https://doi.org/10.1038/35086520 (2001).
3. Runov, A. *et al.* Current sheet structure near magnetic X-line observed by cluster. *Geophys. Res. Lett.* **30**, 1579. https://doi.org/10.1029/2002GL016730,11 (2003).
4. Baumjohann, W. *et al.* Characteristics of high-speed ion flows in the plasma sheet. *J. Geophys. Res.* **95**, 11507–11520. https://doi.org/10.1029/JA095iA04p03801 (1990).
5. Angelopoulos, V. *et al.* Bursty bulk flows in the inner central plasma sheet. *J. Geophys. Res.* **97**(A4), 4027–4039. https://doi.org/10.1029/91JA02701 (1992).
6. Zhang, L. Q. *et al.* X line distribution determined from earthward and tailward convective bursty flows in the central plasma sheet. *J. Geophys. Res.* **115**, A06218. https://doi.org/10.1029/2009JA014429 (2010).
7. Øieroset, M., Phan, T. D., Fujimoto, M. & Lin, R. P. Distant magnetotail reconnection and the coupling to the near-Earth plasma sheet: Wind and geotail case study. *Geophys. Res. Lett.* **31**, L18805. https://doi.org/10.1029/2004GL020321 (2004).
8. Troshichev, O. A., Kokubun, S., Kamide, Y., Mukai, T. & Yamamoto, T. Fast earthward plasma flows observed in the mid/distant tail under quiet conditions: Relation to substorms. *Geophys. Res. Lett.* **26**, 643–646. https://doi.org/10.1029/1999GL900079 (1999).
9. Angelopoulos, V. *et al.* Statistical characteristics of bursty bulk flow events. *J. Geophys. Res.* **99**(A11), 21257–21280. https://doi.org/10.1029/94JA01263 (1994).
10. Cao, J. B. *et al.* Joint observations by cluster satellites of bursty bulk flows in the magnetotail. *J. Geophys. Res.* **111**, A04206. https://doi.org/10.1029/2005JA011322 (2006).
11. Baumjohann, W. Modes of convection in the magnetotail. *Phys. Plasmas* **9**, 3665–3667. https://doi.org/10.1063/1.1499116 (2002).
12. Zhang, L. Q. *et al.* Parallel-dominant and perpendicular-dominant components of the fast bulk flows: Comparing with the PSBL beams. *J. Geophys. Res. Space Phys.* https://doi.org/10.1002/2015JA021669 (2015).
13. Zhang, L. Q. *et al.* Turbulent current sheet frozen in bursty bulk flow: Observation and model. *Sci. Rep.* https://doi.org/10.1038/s41598-022-19266-6 (2022).
14. Shiokawa, K. *et al.* Braking of high-speed flows in the near-Earth tail. *Geophys. Res. Lett.* **24**, 1179–1182. https://doi.org/10.1029/97GL01062 (1997).
15. Zhang, L. Q. *et al.* BBF deceleration down-tail of X < −15 RE from MMS observation. *J. Geophys. Res. Space Phys.* **125**, e20190JA26837. https://doi.org/10.1029/2019JA026837 (2020).
16. Vörös, Z. *et al.* Magnetic turbulence in the plasma sheet. *J. Geophys. Res.* **109**, A11215. https://doi.org/10.1029/2004JA010404 (2004).
17. Zelenyi, L., Artemyev, A. & Petrukovich, A. Properties of magnetic field fluctuations in the Earth's magnetotail and implications for the general problem of structure formation in hot plasmas. *Space Sci. Rev.* https://doi.org/10.1007/s11214-014-0037-7 (2014).
18. Zimbardo, *et al.* Magnetic turbulence in the geospace environment. *Space Sci. Rev.* **156**, 89–134. https://doi.org/10.1007/s11214-010-9692-5 (2010).
19. Weygand, J. M. *et al.* Plasma sheet turbulence observed by cluster II. *J. Geophys. Res.* **110**, A01205. https://doi.org/10.1029/2004JA010581 (2005).

20. Angelopoulos, V. *et al.* Plasma sheet electromagnetic power generation and its dissipation along auroral field lines. *J. Geophys. Res.* **107**(A8), 1181. https://doi.org/10.1029/2001JA900136 (2002).
21. Chaston, C. C., Bonnell, J. W., Clausen, L. & Angelopoulos, V. Correction to "Energy transport by kinetic-scale electromagnetic waves in fast plasma sheet flows". *J. Geophys. Res.* **117**, A12205. https://doi.org/10.1029/2012JA018476 (2012).
22. Wang, T., Cao, J., Fu, H., Meng, X. & Dunlop, M. Compressible turbulence with slow-mode waves observed in the bursty bulk flow of plasma sheet. *Geophys. Res. Lett.* **43**, 1854–1861. https://doi.org/10.1002/2016GL068147 (2016).
23. Cho, J. & Lazarian, A. Generation of compressible modes in MHD turbulence. *Theor. Comput. Fluid Dyn.* **19**(2), 127–157. https://doi.org/10.1007/s00162-004-0157-x (2005).
24. Borovsky, J. E., Elphic, R. C., Funsten, H. O. & Thomsen, M. F. The Earth's plasma sheet as a laboratory for flow turbulence in high-β MHD. *J. Plasma Phys.* **57**, 1. https://doi.org/10.1017/S0022377896005259 (1997).
25. Borovsky, J. E. & Funsten, H. O. MHD turbulence in the Earth's plasma sheet: Dynamics, dissipation, and driving. *J. Geophys. Res.* **108**(A7), 1284. https://doi.org/10.1029/2002JA009625 (2003).
26. De Spiegeleer, A. *et al.* Low-frequency oscillatory flow signatures and high-speed flows in the Earth's magnetotail. *J. Geophys. Res Space Phys.* **122**, 7042–7056. https://doi.org/10.1002/2017JA024076 (2017).
27. Hones, E. W. Jr. *et al.* Vortices in magnetospheric plasma flow. *Geophys. Res. Lett.* **5**, 1059–1062. https://doi.org/10.1029/GL005i012p01059 (1978).
28. Tian, A. M. *et al.* A series of plasma flow vortices in the tail plasma sheet associated with solar wind pressure enhancement. *J. Geophys. Res.* **115**, A09204. https://doi.org/10.1029/2009JA014989 (2010).
29. Zhang, L. Q., Baumjohann, W., Dai, L., Khotyaintsev, Y. V. & Wang, C. Measurements of the vorticity in the bursty bulk flows. *Geophys. Res. Lett.* **46**, 10322–10329. https://doi.org/10.1029/2019GL084597 (2019).
30. Zhang, L. Q. *et al.* Anisotropic vorticity within bursty bulk flow turbulence. *J. Geophys. Res. Space Phys.* **125**, e2020JA028255. https://doi.org/10.1029/2020JA028255 (2020).
31. Zhang, L. Q. *et al.* Vorticity within bursty bulk flows: Convective versus kinetic. *J. Geophys. Res. Space Phys.* **127**, e2020JA028934. https://doi.org/10.1029/2020JA028934 (2022).
32. Russell, C. T. *et al.* The magnetospheric multiscale magnetometers. *Space Sci. Rev.* **199**, 189–256. https://doi.org/10.1007/sl1214-014-0057-3 (2016).
33. Pollock, C. *et al.* Fast plasma investigation for magnetosphere multiscale. *Space Sci. Rev.* **199**, 331–406. https://doi.org/10.1007/s11214-016-0245-4 (2016).
34. Torbert, R. B. *et al.* The FIELDS instrument suite on MMS: Scientific objectives, measurements, and data products. *Space Sci. Rev.* **199**, 105–135. https://doi.org/10.1007/s11214-014-0109-8 (2016).
35. Lindqvist, P.-A. *et al.* The spin-plane double-probe electric field instrument for MMS. *Space Sci. Rev.* **199**, 137–165. https://doi.org/10.1007/s11214-014-0116-9 (2014).
36. Turkakin, H., Mann, I. R. & Rankin, R. Kelvin–Helmholtz unstable magnetotail flow channels: Deceleration and radiation of MHD waves. *Geophys. Res. Lett.* **41**, 3691–3697. https://doi.org/10.1002/2014GL060450 (2014).
37. Birn, J., Raeder, J., Wang, Y. L., Wolf, R. A. & Hesse, M. On the propagation of bubbles in the geomagnetic tail. *Ann. Geophys.* **22**(5), 1773–1786. https://doi.org/10.5194/angeo-22-1773-2004 (2004).
38. Sundkvist, D. *et al.* In situ multi-satellite detection of coherent vortices as a manifestation of Alfvénic turbulence. *Nature* **436**, 825–828. https://doi.org/10.1038/nature03931 (2005).
39. Shebalin, J. V., Montgomery, D. C. & Matthaeus, W. H. Anisotropy in MHD turbulence due to a mean magnetic field. *J. Plasma Phys.* **29**, 525 (1983).
40. Schertzer, D., Lovejoy, S., Schmitt, F., Chigirinskaya, Y. & Marsan, D. Multifractal cascade dynamics and turbulent intermittency. *Fractals* **05**, 427–471. https://doi.org/10.1142/S0218348X97000371 (1997).
41. Wan, M. *et al.* Intermittent dissipation and heating in 3D kinetic plasma turbulence. *Phys. Rev. Lett.* **114**(17), 175002. https://doi.org/10.1103/PhysRevLett.114.175002 (2015).
42. Huang, S. Y. *et al.* Intermittent dissipation at kinetic scales in the turbulent reconnection outflow. *Geophys. Res. Lett.* **49**, e2021GL096403. https://doi.org/10.1029/2021GL096403 (2022).
43. Goldstein, M. L., Roberts, D. A. & Matthaeus, W. H. Magnetohydrodynamic turbulence in the solar wind. *Ann. Rev. Astron. Astrophys.* **33**, 283 (1995).
44. Parashar, T. N. & Matthaeus, W. H. Propinquity of current and vortex structures: Effects on collisionless plasma heating. *Astrophys. J.* **832**, 57 (2016).
45. Politano, H., Pouquet, A. & Sulem, P. L. Current and vorticity dynamics in three-dimensional magnetohydrodynamic turbulence. *Phys. Plasmas* **2**, 2931–2939. https://doi.org/10.1063/1.871473 (1995).
46. Treumann, R. A., Wolfgang, B. & Yasuhito, N. Ideal MHD turbulence: The inertial range spectrum with collisionless dissipation. *Front. Phys.* https://doi.org/10.3389/fphy.2015.00022 (2015).
47. Philipp, G., O'Shea, B. W. & Beckwith, K. As a matter of tension: Kinetic energy spectra in MHD turbulence. *Astrophys. J.* https://doi.org/10.3847/1538-4357/abdd22 (2021).

Acknowledgements

Author contributions

Professor L.Q.Z., C.W., R.S.W., and W.B. wrote the main manuscript text. Professor J.L.B. and Y.V.K. check the data. Professor L.Q.Z. and J.Y.W. prepared figures in the paper. All authors reviewed the manuscript.

Competing interests

The authors declare no competing interests.

Additional information